Electronic Supplementary Information (ESI) for

Overcoming metal-induced fluorescence quenching on plasmo-photonic metasurfaces coated by a self-assembled monolayer

B. Choi, M. Iwanaga,* H. T. Miyazaki, Y. Sugimoto, A. Ohtake, and K. Sakoda
National Institute for Materials Science, 1-1 Namiki, Tsukuba 305-0044, Japan
*E-mail: iwanaga.masanobu@nims.go.jp

1. Experimental Method

Preparation of stacked complementary (SC) plasmo-photonic (PlasPh) metasurfaces

The SC PlasPh metasurfaces were made on silicon-on-insulator (SOI) substrates, which contained three layers: the top layer was Si single-crystal layer of 200 nm thickness, the middle buried oxide (BOX) layer of 400 nm thickness, and the bottom layer was Si wafer of about 600 μm thickness.

The details of ultraviolet nanoimprint procedure were similar to that described in our previous report [1]. In this study, we conducted lateral structure tuning that used only one quartz mold and varied different air-hole diameters of the Si photonic crystal slabs. The structural tuning was made possible by changing the residual resist treatment with O_2 and N_2 mixed gas plasma in the dry etching process [2]. Each substrate has a large-area metasurface of 10×10 mm^2. The metasurfaces consist of three layers: the top perforated Au layer with a thickness of 35 nm, the middle perforated SOI layer, and the bottom Au-disk-embedded SOI layer. The periodicity was fixed at 410.5 nm and air-hole diameter (D) was varied 190 to 315 nm.

SAM growth on the metasurfaces

We carried out an establish protocol to form SAMs [3]. First, we prepared three ethanol solutions of 15-carboxy-1-pentadecanethiol (15-CPDT, DOJINDO Laboratories, Kumamoto, Japan), 10-carboxy-1-decanethiol (10-CDT), and 5-carboxy-1-pentathiol (5-CPT). Each concentration was approximately 1 mM. The substrates including SC PlasPh metasurfaces just after Au deposition were immersed in the solution at 30 °C. Although the Au surface would be fully coated by a SAM in about 15 minutes, we put the substrates for 1 hour to obtain well coverage by the SAM. The substrates were rinsed with ethanol to remove the unbound thiolates, and then dried with N_2 gas.

Figure S1 shows a series of XPS spectra of SAM: (a) and (b) 15-CPDT; (c) and (d) 10-CDT; (e) and (f) 5-CPT. The SAMs were grown on SC metasurfaces of D 260 nm. Measured XPS signals are shown with black solid lines and the fitted curves using Voigt functions with red dashed lines. The spectral shapes of Au and S in Figure S1 are similar in each atom. The integrated ratio of S $2p$ (right-hand side) to Au $4f$ states (left-hand side) were estimated to be $(6.4 \pm 2.0) \times 10^{-3}$ for 15-CPDT, $(7.4 \pm 1.3) \times 10^{-3}$ for 10-CDT, and $(6.3 \pm 0.8) \times 10^{-3}$ for 5-CPT. As noted in the text, a SAM grown on flat Au(111) surface shows that the ratio of S $2p$ to Au $4f$ signals is 6.2×10^{-3} [4]. Therefore, it is most likely that the SAM fully covers the outmost Au surface on the SC metasurface.

We also note the procedure for repeated usage of the SC metasurfaces. When a different SAM was formed on a SC metasurface, the 35-nm-thick Au films were removed from the SC metasurfaces and then Au films were re-deposited on the nanoimprinted SOI substrates.
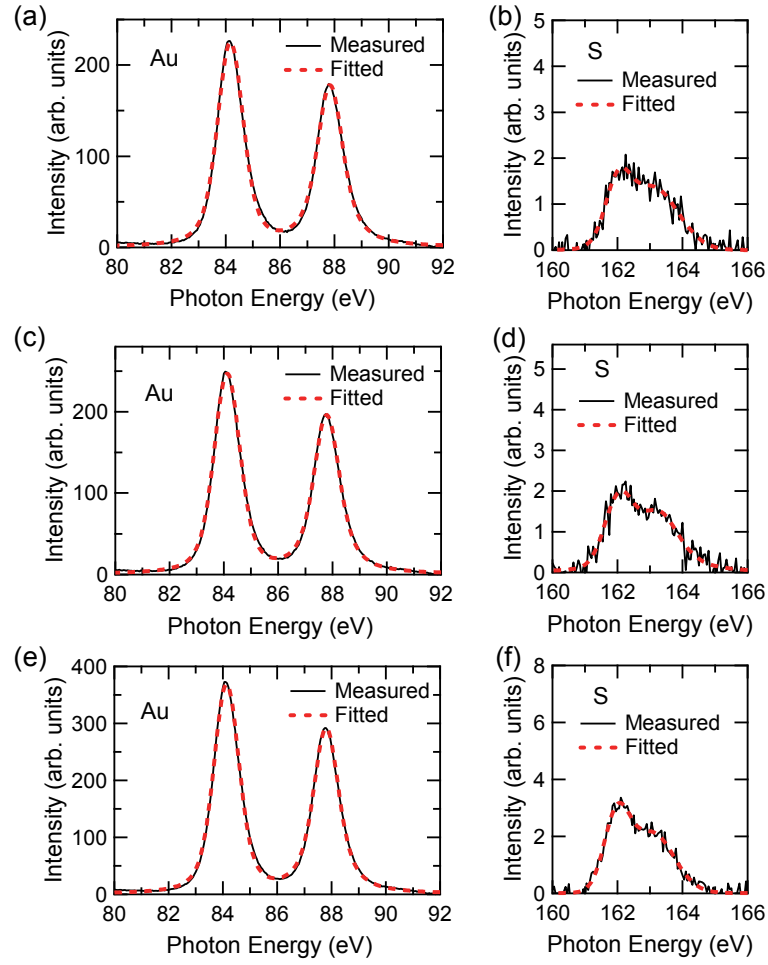
Figure S1. Measured XPS spectra of Au 4*f* (left-hand side) and S 2*p* (right-hand side) states from the SAMs on SC metasurfaces of D 260 nm. (a) and (b) 15-CPDT. (c) and (d) 10-CDT. (e) and (f) 5-CPT. Black solid lines denote measured data. Red dashed lines represent fitted curves using Voigt functions.

Reflectance (R) measurement

Figure S2 shows a series of measured R spectra of the SC metasurfaces of D 190 to 315 nm. The R spectrum of D 265 nm is shown again for readers' convenience. The fourth (▲) and sixth (●) resonances are marked. As the air-hole diameter D becomes larger, the two resonances shift to shorter wavelengths.

The R spectra were measured using a spectrometer that is able to vary incident angles and polarizations. We show R spectra at incident angle of 5° and *x* polarization; the *xy* coordinate is defined in Fig. 2(b) and the plane of incidence was set to *xz* plane where the *z* axis is defined to be perpendicular to the *xy* plane. In the setting, the *x* polarization corresponds to *p* polarization.
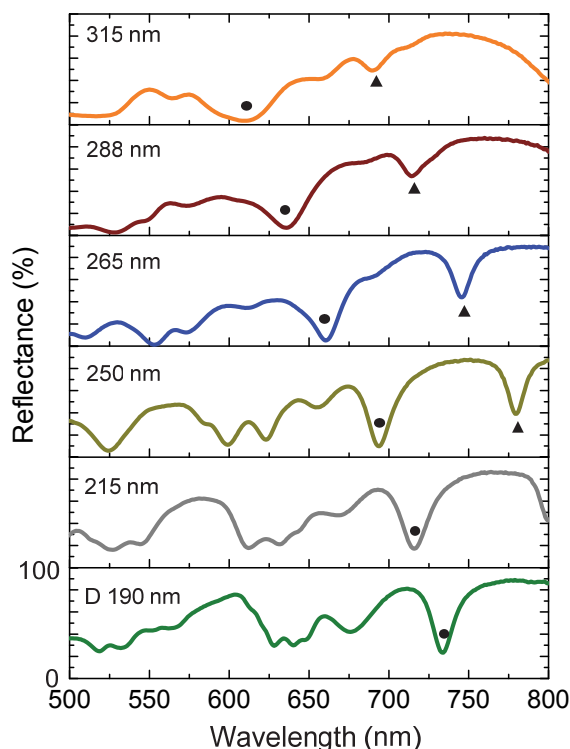
Figure S2. A series of measured R spectra of the SC metasurfaces of D 190 to 315 nm. Each R spectrum is shown in the 0–100% scale. The fourth (▲) and sixth (●) resonances are shown with the marks. The incident angle was 5°. The incident polarization was *x* polarization; the *x* axis is defined in Fig. 2(b).

Enhanced fluorescence (FL) spectra measurement

We measured FL signals of rhodamine 590 (R590, Exciton Inc., Ohio, USA) molecules on the SC metasurfaces and on reference Si wafer substrate. The setup of the FL measurement was illustration-and-collection configuration at the normal incidence. The molecules were adsorbed on the metasurfaces with/without SAM by immersing the metasurface substrates in R590 methanol solutions of 500 nM for 30 s.

In the sequence of FL measurement, the dispersed R590 molecules can be successfully removed from the metasurfaces by immersing them in N-methylpyrrolidone (NMP) solution at 80°C and rinsing them by ethanol. We assume that the position of molecules was randomly distributed over the whole SC metasurfaces. The FL signals were induced by continuous-wave laser light of 532 nm that was focused to an approximate 25-μm-diameter beam spot, and were collected using a objective lens with numerical aperture 0.4 at the normal incidence configuration. The pump power was 250 μW on the sample surfaces. The FL signals were measured after photo-irradiation for 3 minutes to avoid photo-breaching effects of the R590 molecules and to keep the FL signals almost constant during the measurement time of 20 s.

Figure S3 shows enhanced FL spectra of R590 on the SC metasurfaces of D 190, 215, 250, 265, 288 and 315 nm. Each panel in Figure S3 shows three measured cases: (1) SAM of 10-CDT was formed (light green), (2) SAM of 15-CPDT was formed (blue), (3) without the SAM (black). In all the SC metasurfaces, the SAM-covering metasurfaces exhibited better FL enhancement by 10 to 100 times. We note that the peaks of the enhanced FL spectra correspond to the R dip in Figure S2. For example, in case of D 190 nm, the FL peaks appear at 630 nm and R dips also appear around 630 nm as shown in Figure S2. Similar correspondences are easily verified in other

SC metasurfaces of different D. Note that the R dips correspond to emittance peaks, due to Kirchhoff's law [5] as described in the text.

Figure S3 also shows that SAMs of 10-CDT work well for larger FL signals from the SC metasurfaces of D 190, 215, 250, 265, 288 and 315 nm, whereas SAMs of 15-CPDT are good for the SC metasurfaces of D 250 and 265 nm. Thus, the selection of SAMs is an option to prepare good FL- enhancing platforms. The enhanced FL peaks are consistent with the dips of R spectra in Figure S2 (or the peaks of absorption), indicating that the enhanced wavelength ranges can be tuned by selecting a proper D.
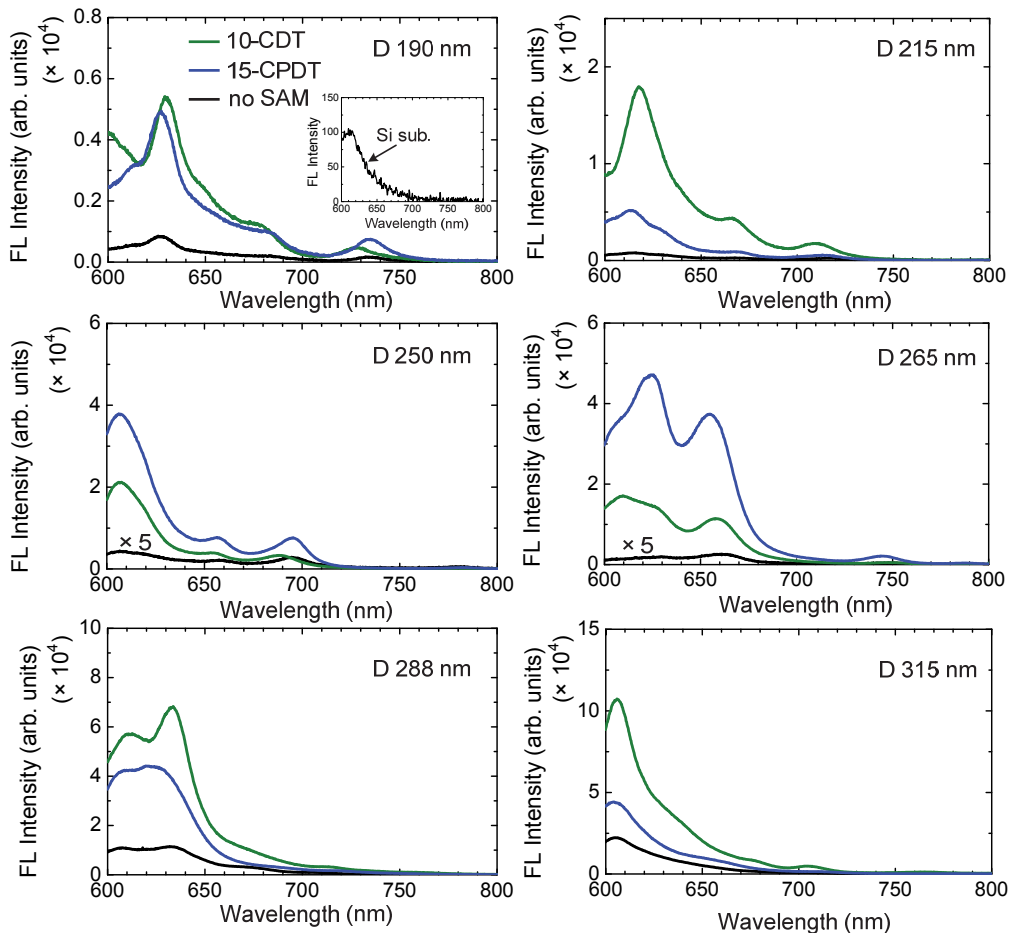

Figure S3. Enhanced FL spectra of R590 on the SC metasurface of D 190 to 315 nm. Green and blue curves denote enhanced FL spectra from the SC metasurfaces with 10-CDT and 15-CPDT SAMs, respectively. Black curves denote enhanced FL spectra from the SC metasurfaces without SAMs. The inset in the panel for D 190 nm shows FL spectrum of R590 molecules on a Si substrate in an equivalent measurement.

Figure S4 shows a series of FL enhancement factors (EFs) for various D from 190 to 315 nm. The EFs were evaluated from the FL spectra in Figure S3. The reference was set to FL spectrum on the Si substrate. The result on the SAM of 15-CPDT was picked up. The most prominent peak of EF appears at 660 nm in case of D 265 nm and is close to 2000-fold. Note that the peak corresponds to the R dip that takes nearly 0%, which implies nearly 100% emittance of the SC metasurface at the wavelengths [5]. The R spectrum of D 265 nm is shown with blue dashed curve and plotted for the right axis. The EF peak over 1000-fold is also observed for D 250 nm (dark yellow curve).
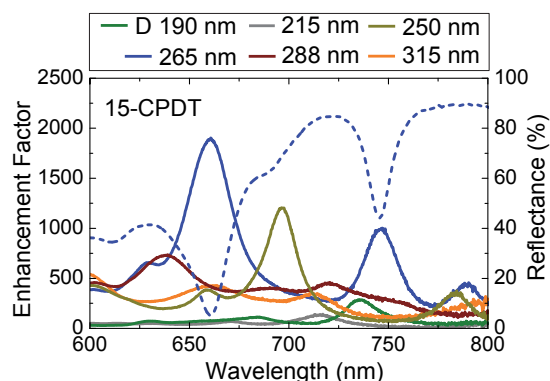
Figure S4. Enhancement factor (EF), based on Figure S3, for various air-hole diameter (D) from 190 to 315 nm. The SAM was 15-CPDT. The measured R spectrum is shown with blue dashed line for D 265 nm and plotted for the right axis.

Figure S5 compiles FL EFs (closed circles with solid lines) with error bar and absorbance, A, (open circles with dashed lines) on the sixth resonance. The A spectrum was evaluated from the measured R spectra in Figure S2. The EF is plotted for the left axis and the A is plotted for the right axis. Qualitatively, the increase in the A is consistent with the increase in the EF. We note that, as the diameter is larger than 265 nm, the A at the range less than 650 nm includes a larger loss by the constituent materials (i.e. Au and Si). The absorption loss in bulk materials is not necessarily linked to emittance [5]; we therefore infer that a deviation was observed from 600 to 650 nm.

Figure S5 provides useful information on how to select a proper metasurface for FL sensing. If one needs to conduct FL sensing at 660 nm for a particular species of molecules, the most suited metasurface is that of D 265 nm. Thus, the series of the SC metasurfaces is able to meet on-demand FL sensing. The choise of SAM is, of course, an option.
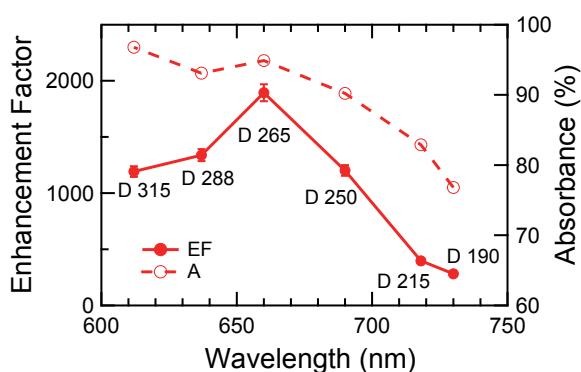

Figure S5. Correlation of EFs (closed circles with solid lines) with absorbance A (open circles with dashed lines), which was collected from Figure S4. The EFs were taken at the sixth resonance indicated by the closed circle in Figure 2(d). The air-hole diameters, D, are specified in nm.

Figure S6 shows EFs of R590 on the SC metasurfaces without the SAM. The EF spectra were compiled from Figure S4. The air-hole diameter D was varied from 190 to 315 nm. The EF spectra have the maximum values in the range from several tens to a few hundreds. These results are consistent with a previous report [1].
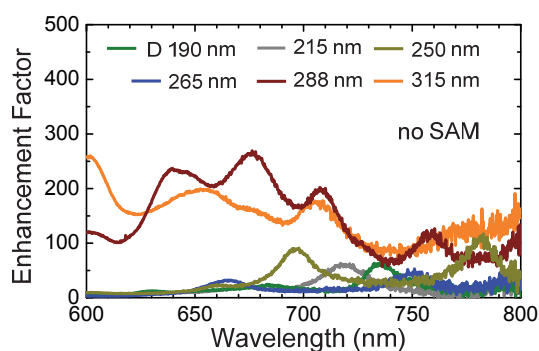
5

Figure S6. Enhanced FL spectra of R590 on the SC PlasPh metasurfaces without any SAM. The air-hole diameters D were varied from 190 to 315 nm.

FL decay time measurement

We measured FL decay of R590 molecules to obtain information on the decay rate. Figure S7(a) shows measured normalized extinction (black) and FL (green) spectra of R590 methanol solution of 500 nM. The extinction peak is located at 528 nm and the FL peak at 547 nm. The FL spectrum was induced under photo-excitation at 446 nm. The FL quantum yield was also measured using an integration sphere under excitation at 530 nm and was estimated to be 91%, which is a typical value of rhodamine dyes.

Figure S7(b) and 7(c) display measured FL decay curves (blue) observed at 555 and 663 nm, respectively. Both decay curves were well fitted by a single exponential curve (red) and had decay time τ of approximately 4.0 ns. Because the quantum yield was over 90%, the radiative decay is dominant and responsible for the decay time. Thus, the radiative decay time of R590 molecules in methanol solution was found to be 4.0 ns.

In the decay measurement, the incident laser pulses of 446 nm had 2 ps temporal width and the temporal resolution of the detection system was approximately 60 ps. Further details in the measurement were similar to the experiment reported in [6].
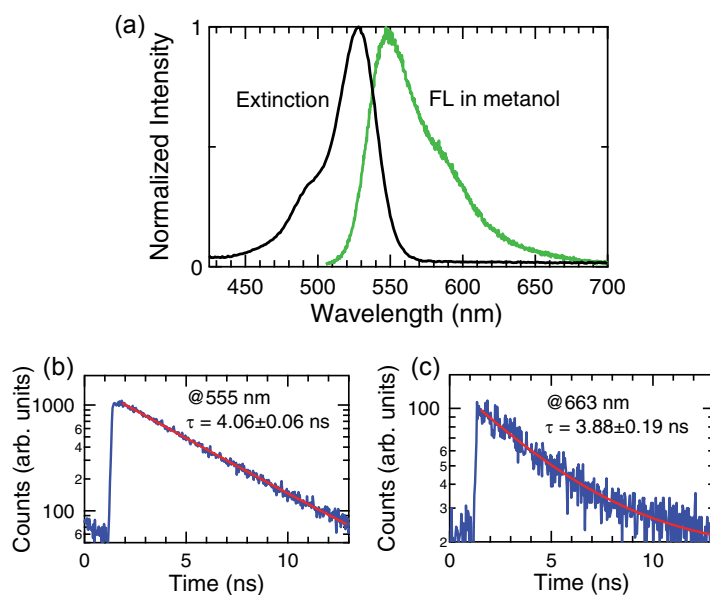

Figure S7. (a) Normalized extinction (black) and FL (green) spectra of R590 methanol solution of 500 nM. (b) and (c) Measured FL decay curves (blue) and single-exponential fittings (red) at 555 and 663 nm, respectively.

Figure S8(a) shows FL spectrum of R590 located on a SAM-coated SC metasurface of D 260 nm. The SAM was 15-CPDT. The spectral shape is quite similar to that in Figure 3(a). Figure S8(b) and S8(c) present FL decay curves (blue line with closed circles) observed at 555 and 663 nm, respectively. The wavelengths are indicated by arrows in Figure S8(a). The major parts of the decay curves were fitted by single exponential curves (red) and were found to have decay time $\tau \approx$ 0.35 ns. The decay time is 11-fold shorter than the radiative decay time in Figure S7. The experimental setup was same to that for Figure S7. Note that it is undefinite whether the decay in Figure S8(b) and S8(c) comes from radiative or nonradiative (NR) component.

In this case, FL quantum yield was also measured and found to be under the detection limit (i.e. 0.1%) in the measurement incorporating the integration sphere; therefore it is very difficult to identify the origin of the decay time τ. This result on the FL yield is reasonable because the number of R590 molecules involved in the measurement was far less than that in the methanol solution.
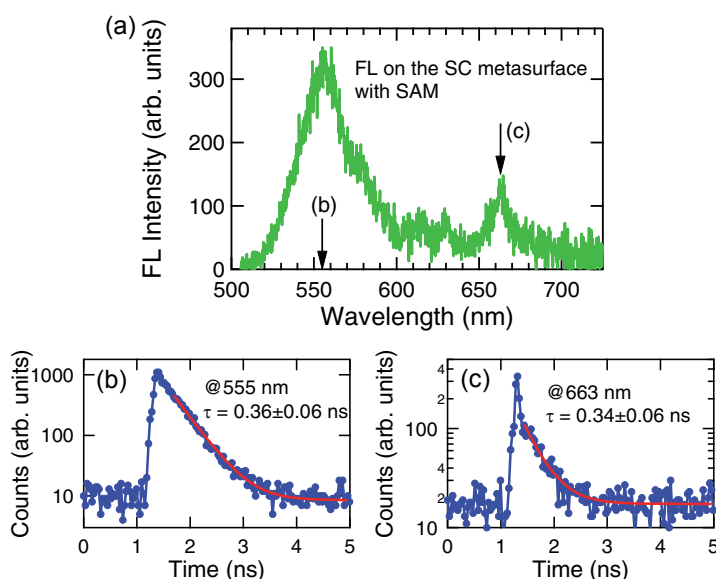

Figure S8. (a) FL spectra of R590 molecules on a SAM-coated SC metasurface of D 260 nm. The excitation wavelength was 446 nm. (b) and (c) FL decay curves (blue line with closed circles) observed at 555 and 663 nm (arrows in (a)), respectively. Red curves represent fitted single exponential curves.

We here note that the FL decay on the SC metasurfaces without SAMs and on the reference Si substrates was not measurable in the measurement setup. This was because the signal-to-noise ratio in the FL decay measurement was less than 10^2 and the FL intensities from the SC metasurfaces with SAMs and from the Si substrate are several tens fold weaker than the FL intensity from the SAM-coated SC metasurface shown in Figure S8. Thus it was not possible to compare the experimental data on the decay time in Figure S8 with those from the reference.

FL spectra of R590 molecules on flat surfaces

Figure S9 displays FL spectra of R590 on a flat Si wafer substrate (black line), a Au film on a Si substrate (orange line) and a SAM-coated Au film on a Si substrate (red broken line). The SAM was 15-CPDT. It was confirmed that the FL was observed in a similar amount from the Si substrate and the SAM-coated Au film on a Si substrate, suggesting that surface absorption capability is similar on the two flat surfaces. Quantitatively, the FL intensity from the SAM-coated Au film is about 2 times weaker than the FL intensities from the Si wafer.
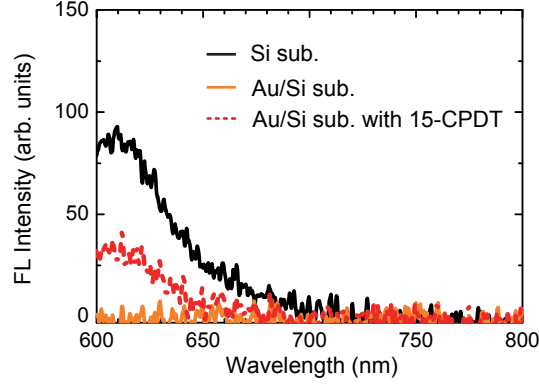
Figure S9. FL spectra of D590 on flat surfaces. A Si wafer substrate (black line), a SAM-grown Au thin film on Si substrate (red broken line) and a Au-film-deposited Si substrate (orange line) were tested. The SAM was 15-CPDT.
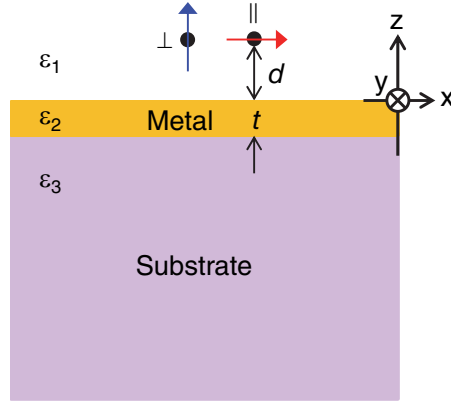

Figure S10. Illustration of dipoles (dots) near the flat surface, which are located at a distance d. The polarization of the dipoles has two orientations (i.e. perpendicular $\perp$ and parallel $\|$).

As for decay rate in configurations composed of flat interfaces, a comprehensive study was reported in 1970s [7]. Following the analysis based on a classical model for damping oscillator, we evaluated decay rates of FL molecules on/near flat surfaces. In a configuration including thin metallic film in Figure S10, total decay rate b_{tot} is written as follows [7]:

$$b_{\text{tot}} = \frac{1}{3}b^{\perp} + \frac{2}{3}b^{\|} \tag{1}$$

$$b^{\perp} = q - \frac{3}{2}q \, \text{Im} \int_0^{\infty} R_p \exp(2l_1 k_1 d) \frac{u^3 du}{l_1} + (1-q) \tag{2}$$

$$b^{\|} = q + \frac{3}{4}q \, \text{Im} \int_0^{\infty} [R_s + (1-u^2)R_p] \exp(2l_1 k_1 d) \frac{u \, du}{l_1} + (1-q) \tag{3}$$

where q denotes intrinsic FL quantum yield in a molecule, R_s and R_p are complex reflection coefficient at s and p polarizations, ε_i is relative permittivity in each layer, $l_1 = -i\sqrt{\varepsilon_1 - u^2}$, $k_1 = \sqrt{\varepsilon_1}\omega/c$ (ω: angular frequency of light, c: the velocity of light in vacuum) and d is distance between the dipoles and the top surface. Note that the b_{tot} is averaged regarding perpendicular $b^{\perp}$ and parallel $b^{\|}$ components, represents the whole decay rate in the configuration and contains both

radiative and NR decay rates. The NR term comes from the integrals over $(1,\infty)$ in Eqs. (2) and (3), including energy transfer to the metal film and/or the substrate.
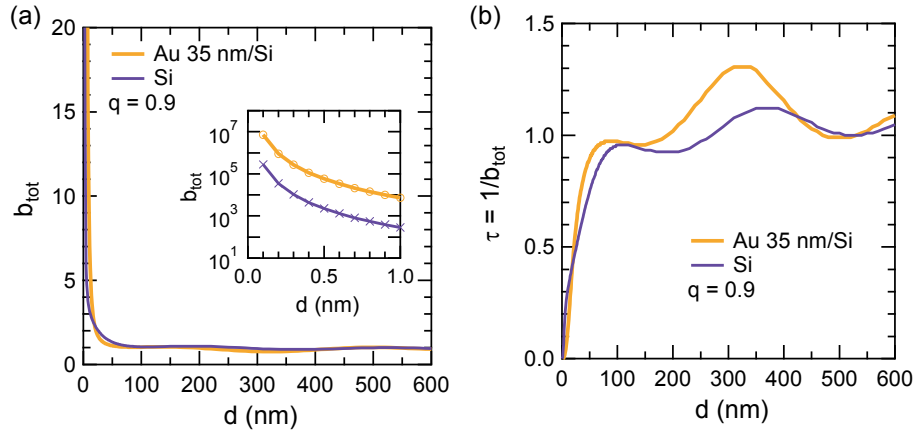

Figure S11. (a) Total decay rate b_{tot} for distance d. Yellow curve denotes b_{tot} in case of dipoles near the flat Au/Si substrate. Purple curve stands for b_{tot} in case of dipole near the Si substrate. The inset enlarges the b_{tot} near $d = 0$. (b) Decay time τ, normalized by q.

Figure S11(a) shows calculated b_{tot} from Eq. (1). The wavelength was set to 620 nm. Two cases were evaluated: one is that dipoles were located near the flat Au/Si substrate (yellow curve), as shown in Figure S10; the other was that dipoles were located near the Si substrate (purple curve). The former assumed Au thickness $t = 35$ nm and the latter assumed $t = 0$ nm. In both cases, when dipoles become close to the surface, the decay rates b_{tot} rapidly increase especially at $d < 50$ nm. The inset shows the b_{tot} at d less than 1.0 nm. The rates b_{tot} take very large values but is not divergent; the ratio of the rates was found to be almost constant. As shown later (Figure S11), the increase in the b_{tot} is dominantly due to the increase in the NR component. It deserves noting that the increase in the NR decay rates takes place not only near the metallic surface but also near the Si surface. Permittivity of Au and Si was taken from literature, which is cited in the text.

Figure S11(b) shows decay time τ, defined by $1/b_{tot}$. Note that the decay time is normalized by intrinsic decay time $1/q$. As the rates b_{tot} significantly increase, the decay time rapidly becomes small at $d < 50$ nm. These kinds of behaviour were experimentally confirmed in many examples [7].
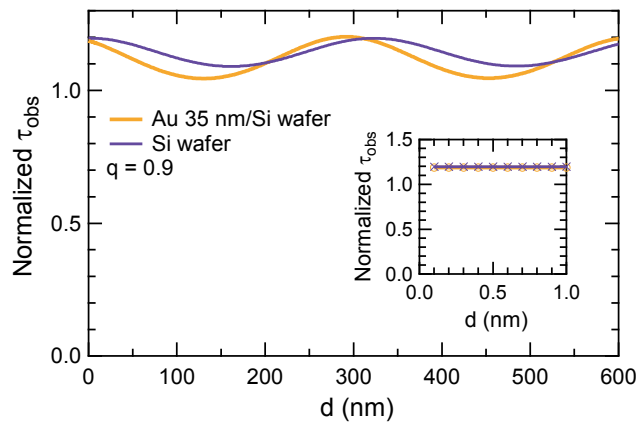

Figure S12. Radiative decay times extracted from the total decay rates b_{tot}, presented in a similar manner to Figure S11(b). The inset magnifies a range of d near 0 nm.

9

Figure S12 shows radiative decay times of dipoles near the flat Au 35 nm/Si substrate (yellow) and near the Si substrate (purple). The radiative decay times were evaluated in the measurement configuration using an objective lens of numerical aperture 0.4; therefore, the integrals in Eqs. (2) and (3) were calculated for a range of (0,0.4). Also, radiative decay rate was decomposed in accordance with the Poynting vector for the ±z direction [7]. The +z component was taken because it is observed in the experiment. Obviously, the radiative decay times do not exhibit any definite decrease near $d = 0$ nm and keep almost the intrinsic decay time that is defined by $1/q$. We mention that this tendency remains when we evaluated the integrals over a u-range (0,1), which is responsible for the full radiative contributions.

Summing up Figures S11 and S12, the significant change in b_{tot} comes from the configuration of dipole setting near the flat surfaces and is associated with the growing of NR decay rate; in contrast, radiative decay rate is almost unaffected.

Let us go back to Figure S9. Considering NR decay rates on the two flat surfaces (i.e. the Si substrate and the SAM-coated Au film), the Si substrate has larger NR decay rate and allows small FL quantum yield; therefore, it is likely that larger number of R590 molecules is attached on the Si substrate. Thus it is possible that EF in Figures 3 and S4 takes at least 2-fold larger values though we did not add the incremental factor because precise estimation of the attached molecules is extremely difficult.

The data in Figure S9 were used to consider a relevant reference substrate. We used the Si wafer as the reference as noted in the text. The flat Au surface was unsuited as reference because FL signals were hardly observed.

At the end, we refer to preparation of Au films. The flat Au surfaces and the SAM-coated flat Au surfaces were prepared by depositing Au and growing the SAM at most one day before the FL measurement and were used in a fresh condition. As far as we kept the fresh condition, we observed equivalent FL spectra in all the measurements. When the Au deposition was done more than a month ago, we found apparent deviations of FL signals and excluded such sample from this study.

2. Numerical Method

Calculations for EM fields

We implemented numerical calculations for EM fields in the SC PlasPh metasurfaces by rigorous coupled-wave analysis (RCWA) method as described in the text. Figure S13 presents calculated |**E**| distribution at the excitation wavelength of 532 nm for Figures 3 and S3. The incidence of x polarization was set to travel from the domain above the top xy section and illuminate the top SC metasurface normally. The hot spots appear at the Au/SOI interface in the air holes.
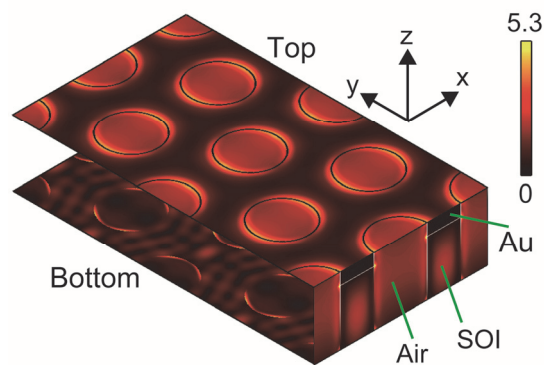
Figure S13. |**E**| distribution at 532 nm calculated for the SC metasurface of D 250 nm. The incidence was set to be |**E**|=1.0.

References

[1] B. Choi, M. Iwanaga, H. T. Miyazaki, K. Sakoda and Y. Sugimoto, J. Micro/Nanolith. MEMS MOEMS, 2014, **13**, 023007.

[2] M. Iwanaga, B. Choi, H. T. Miyazaki, Y. Sugimoto, and K. Sakoda, J. Nanomater., 2015, **2015**, 507656.

[3] Available at http://www.dojindo.com/Shared/Protocol/SAM_Protocol.pdf

[4] M. Kawasaki, T. Sato, T. Tanaka, and K. Takao, Langmuir, 2000, **16**, 1719.

[5] J-J. Greffet and M. Nieto-Vesperinas, J. Opt. Soc. Am. A, 1998, **15**, 2735.

[6] T. Kuroda, K. Fujii and K. Sakoda, J. Phys. Chem. C, 2009, **114**, 983.

[7] R. R. Chance, A. Prock and R. Silbey, Adv. Chem. Phys. 1978, **37**, 1.